Title: The effect of titanium excess and deficiency on the microstructure and dielectric properties of lanthanum doped $Ba_{0.55}Sr_{0.45}TiO_3$ with colossal permittivity

Authors: Kari Nurmi, Heli Jantunen, Jari Juuti

PII: S0955-2219(18)30760-X
DOI: https://doi.org/10.1016/j.jeurceramsoc.2018.12.039
Reference: JECS 12244

To appear in: *Journal of the European Ceramic Society*

Received date: 18 October 2018
Revised date: 18 December 2018
Accepted date: 18 December 2018

Please cite this article as: Nurmi K, Jantunen H, Juuti J, The effect of titanium excess and deficiency on the microstructure and dielectric properties of lanthanum doped $Ba_{0.55}Sr_{0.45}TiO_3$ with colossal permittivity, *Journal of the European Ceramic Society* (2018), https://doi.org/10.1016/j.jeurceramsoc.2018.12.039

The effect of titanium excess and deficiency on the microstructure and dielectric properties of lanthanum doped $Ba_{0.55}Sr_{0.45}TiO_3$ with colossal permittivity

Kari Nurmi[a], Heli Jantunen[a], Jari Juuti[a]

[a] Microelectronics Research Unit, Faculty of Information Technology and Electrical Engineering, University of Oulu, P.O. Box 4500, FIN-90014 Oulu, Finland, E-mail: kari.nurmi@oulu.fi, tel. +358294487961

ABSTRACT

The temperature dependent dielectric properties of $(Ba_{0.54875}Sr_{0.44875}La_{0.0025})Ti_{(1+x)}O_3$ with both an excess and a deficiency of 0.25 mol.% TiO_2 were investigated. The samples were prepared by the mixed oxide method and sintered in a conventional oven at temperatures ranging from 1400 °C to 1475 °C. The cubic perovskite structure was confirmed with XRD at room temperature. The sample with an excess of 0.25 mol.% Ti exhibited reduced grain growth while abnormal grain growth was observed for samples without Ti modification. Samples exhibited colossal permittivity for all modified compositions. With a 0.25 mol.% deficiency of Ti a permittivity over 65,000 and a tan δ under 0.05 were measured over a temperature range of -68 °C to 150 °C and a frequency range between 50 kHz and 1 MHz. This paper shows that by fine tuning the composition, materials with new, exciting and widely adjustable dielectric properties can be achieved.

Keywords: Colossal permittivity, BST, Lanthanum, Doping

1. Introduction

In recent years colossal permittivity (>10^4) materials have gained research interest in the field of electro-ceramics. Materials with high permittivity and low dielectric losses are attractive for numerous electrical applications and enable further miniaturization of dielectric components and have the potential for increased energy density in capacitors. Colossal permittivities have been reported for several doped material systems such as TiO_2[1], $BaTiO_3$[2], $CaCu_3Ti_4O_{12}$(CCTO)[3] and Barium Strontium Titanates (BSTs)[4]. Using various novel sintering methods or atmospheric conditions, colossal permittivity has also been observed in systems without specifically added dopants in the case of $BaTiO_3$ [5], $SrTiO_3$ [6] and BST [7]. However, colossal permittivity materials are still hindered by high dielectric losses or poor temperature stability which reduces the possibilities of practical applications.

BST has been widely studied for its high permittivity and widely adjustable Curie temperature (T_c). The paraelectric/ferroelectric state of BST can be tuned to a desired temperature by altering the Ba:Sr ratio. BSTs in the paraelectric state show low losses (<0.01) over a wide temperature range making them feasible for high frequency applications.[8,9] In the BST material family colossal permittivity has previously been observed in lanthanum doped $Ba_{0.67}Sr_{0.33}TiO_3$[4]. The study showed a promising room temperature colossal relative permittivity over 130,000 and a tan δ of 0.068 at 10 kHz with 0.7 at.% addition of lanthanum. It should be noted that the T_c of this Ba:Sr ratio is approximately at room temperature thus maximizing the permittivity, although, not into the colossal scale. Furthermore, at higher temperatures and frequencies the losses rapidly increased. [4] In the case of other lanthanum doped BST compositions: $Ba_{0.60}Sr_{0.30}TiO_3$ [10], $Ba_{0.74}Sr_{0.26}TiO_3$ [11] and $Ba_{0.8}Sr_{0.2}TiO_3$ [12], no colossal permittivity has been observed. $Ba_{0.60}Sr_{0.30}TiO_3$ showed a room temperature permittivity of 2750.2 and tan δ of 0.0137 at 10 kHz with 0.5 mol.% of lanthanum addition i.e. a significantly reduced permittivity (>7000) compared to undoped BST [10]. Both the $Ba_{0.74}Sr_{0.26}TiO_3$ and $Ba_{0.8}Sr_{0.2}TiO_3$ compositions also showed a relative permittivity under 10,000 and a low tan δ < 0.015 at room temperature, depending on the amount of lanthanum and other dopants [11],[12]. It is apparent that the dielectric properties are influenced not only by the Ba:Sr ratio and the amount of lanthanum and other dopants present but also by the various fabrication routes by which the ceramics are prepared [5-7].

In this work 0.25 mol.% lanthanum doped $Ba_{0.55}Sr_{0.45}TiO_3$ was prepared with both an excess and a deficiency of 0.25 mol.% of Ti in order to determine the compositional effects on microstructure and on the colossal permittivity values. A sample of unmodified BST was also prepared for reference.

2. Experimental

$(Ba_{0.54875}Sr_{0.44875}La_{0.0025})Ti_{(1+x)}O_3$ powders were synthesized using the conventional mixed oxide method with x = +0.25 %; 0 and -0.25 %. $BaCO_3$ (Alfa Aesar, 99.8 %, 197.35 g/mol), $SrCO_3$ (Aldrich, 99.9+ %, 147.63 g/mol), TiO_2 (Alfa Aesar, 99.8 %, Rutile min. 97 %, 79.90 g/mol)

and La_2O_3 (Aldrich, 99.9+, 325.81 g/mol) were used as raw materials. These materials were mixed in appropriate amounts in an ethanol (Etax Aa) solution using a Hilscher UP100H ultrasonic mixer to ensure homogeneity. They were then placed into a furnace at 90 °C to dry the powder mixture. The dry powders were lightly crushed using an agate mortar and pestle and sieved using 180 µm mesh. The powders were pressed into 20 mm diameter pellets with an average sample mass of 5 g under 100 MPa and were then calcined for 10 h at 1150 °C. No binder additives were used in this step. The calcined pellets were crushed with a mortar and pestle and sieved through a 180 µm mesh.

The particle size of the calcined powders was measured with a Backman Coulter LS 13 320 laser diffraction particle size analyzer. All three compositions had a mean particle size under 5 µm. A solution of water and 6 wt.% of PVA (Fluka Chemicals) was used as a binder. 2 drops (~0.066 mg) per 0.5 g were added to the powder and mixed in a mortar and pressed into pellets with a piston and 10 mm diameter mould with a pressure of 100 MPa. All the pressed compacts were first held at 550 °C for an hour to burn off the binder and then sintered in 1475 °C for 4 hours. The sintering profile had a heating rate of 3.5 °C/min. The sintered samples were denoted as +Ti025 with 0.25 mol. % excess of Ti, -Ti025 with 0.25 mol.% Ti deficiency and Ti0 without any Ti modification. The pure $Ba_{0.55}Sr_{0.45}TiO_3$ reference sample, denoted as BST, was fabricated using the same methods as the doped samples. The same heating rate and binder burning step was used with the exception of the sintering temperature which was reduced to 1400 °C.

XRD measurements were conducted with a Bruker D8 Discover to confirm the phases of the formed compositions of the sintered samples. Measurements were taken between 2Θ angles of 20˚ and 70˚ with a step size of 0.01˚ and a dwell time of 1 second per step using 1.6 mm and a 0.6 mm divergence slits. The theoretical densities were calculated from XRD data and the bulk densities of the samples were measured with the Archimedes method.

Sintered samples were polished with sandpaper in descending grit sizes from 800 to 2500 and finished with 1 µm diamond suspension (Struers DiaPro Nap B1). Polished samples were heat etched at sintering temperature without dwell time after which the surface microstructure was analyzed and the average grain size was estimated with an optical microscope (Olympus BX 51) and FESEM (Zeiss ULTRA Plus). A thin carbon coating was applied to the samples for the FESEM analysis.

The pellets were polished and electrodes were made using Heraeus DT1402 silver electrode paste which was fired for 20 min at 600 °C. Dielectric measurements were then conducted with an HP 4284A LCR meter from 20 Hz to 1 MHz with a 1 V_{rms} signal at temperatures ranging from -68 to 150 °C. The accuracy of the measurement depends on the sample characteristics and measurement frequency. The mean accuracies and standard deviations were calculated over the whole frequency range and different samples. For all samples the mean permittivity accuracy and standard deviation values were 0.3 % and ±0.5 %, respectively. For the loss, accuracy values were 0.004 and ±0.008 for pure BST and 0.002 and ±0.003 for modified samples, respectively.

3. Results and discussion

Lanthanum has ionic radii of 1.36 Å in the 12 coordination number and 1.032 Å in the 6 coordination number [13]. This suggests that the La^{3+} ions prefer to occupy A-sites in the ABO_3 structure, substituting Ba^{2+} or Sr^{2+} ions which have ionic radii of 1.61 Å and 1.44 Å, respectively, instead of Ti^{4+}ions in the B-site with significantly smaller ionic radii of 0.605 Å.

The XRD spectra for the sintered samples are shown in Figure 1. All sintered samples displayed a typical cubic BST perovskite structure without any observable secondary phases. This suggests that the dopants had merged into the lattice, although the amount was too small to detect. It is noted that the peak intensities varied slightly in the sintered samples. This may have been caused by the distortion of the unit cell [11] or by preferred orientation in the structure [14].

Table 1. Sample densities and average grain sizes.

Sample	Bulk density (g/cm^3)	Relative density (%)	Average grain size (µm)
BST	5.44 ± 0.05	96.56 ± 0.02	56 ± 15
Ti0	5.52 ± 0.05	97.87 ± 0.02	193(3) ± 30
-Ti025	5.45 ± 0.05	96.73 ± 0.02	86 ± 15
+Ti025	5.49 ± 0.05	97.43 ± 0.02	5 ± 2

Bulk densities and average grain sizes of the sintered samples are shown in Table 1. The samples achieved a high density with minimal porosity. The theoretical density was calculated to be 5.634 – 5.64 ± 0.05 g/cm^3 depending on the composition. The Ti0 sample had the highest density of 5.64 ± 0.05 g/cm^3, and the +Ti025 and –Ti025 samples had 5.635 ± 0.05 g/cm^3 and 5.634 ± 0.05 g/cm^3, respectively.

The microstructure of the sintered samples can be seen in Figure 2 a-b. The pure BST sample (Fig. 2a) showed substantial grain growth, with an average grain size of ~56 ± 15 µm, and small areas between the larger grains where finer grains were located (size of a few microns). In the case of the Ti0 sample, i.e. with only La addition, abnormal grain growth was pronounced (Fig. 2b) where large facetted grains grew randomly amongst a fine grain matrix, with bimodal size distribution having an average grain size of 193 ± 30 µm for the larger grains and 3 ± 2 µm for the overall matrix. This suggests a possible liquid phase developing and wetting certain grain boundaries [15]. The -Ti025 sample (Fig. 2c) presented a similar microstructure to the pure BST sample but with a larger average grain size of 86 ± 15 µm and less areas with finer grains. The BST, Ti0 and –Ti025 samples all contained spots from which large grains seemed to be growing, most prominently in the Ti0 samples. The large grains seemed to grow in a similar fashion to that of single crystals that are grown by deliberately adding a composition-inducing liquid phase in the samples [16,17]. On the other hand, the +Ti025 samples (Fig. 2d) displayed a uniform microstructure with moderate grain growth. It is obvious that the excess TiO_2 inhibits the grain growth and makes the structure more homogenous. A closer look at the abnormal grain growth site in Fig. 2c is displayed in the SEM micrographs in Figure 3. EDS analysis confirmed the presence of aluminum. Silicon was also detected in some samples. Aluminum oxide could form a liquid phase with barium oxide at 1425 °C [18] and silicon dioxide even in temperatures as low as 1400 °C [19].

Starting powders inherently contain these elements, and the agate mortar may also have introduced more impurities into the powders. Thus small amount of liquid phase could be formed from these impurities and the base material during the processing of the powders/samples. In addition, compositionally inhomogeneous regions with excessive amounts of certain elements allow a liquid phase to form which can cause such an effect [20]. Figure 4. shows the dielectric properties of the samples at room temperature for different compositions. The BST sample showed stable losses under 0.02 and a relative permittivity greater than 2800 over the whole frequency range. The Ti0 sample had a considerable increase in permittivity and losses due to the

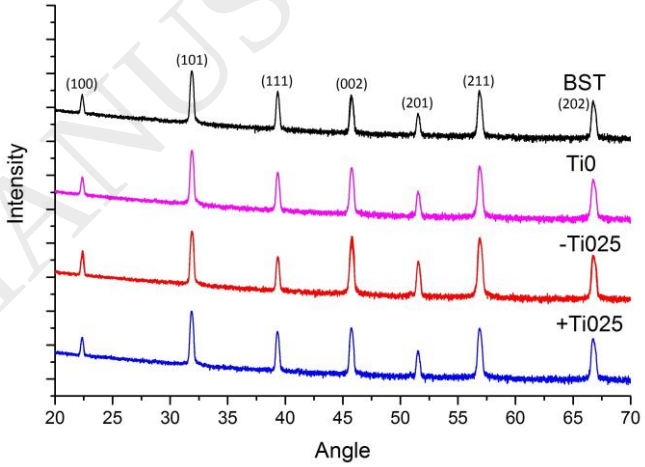

Figure 1. XRD patterns for sintered samples.

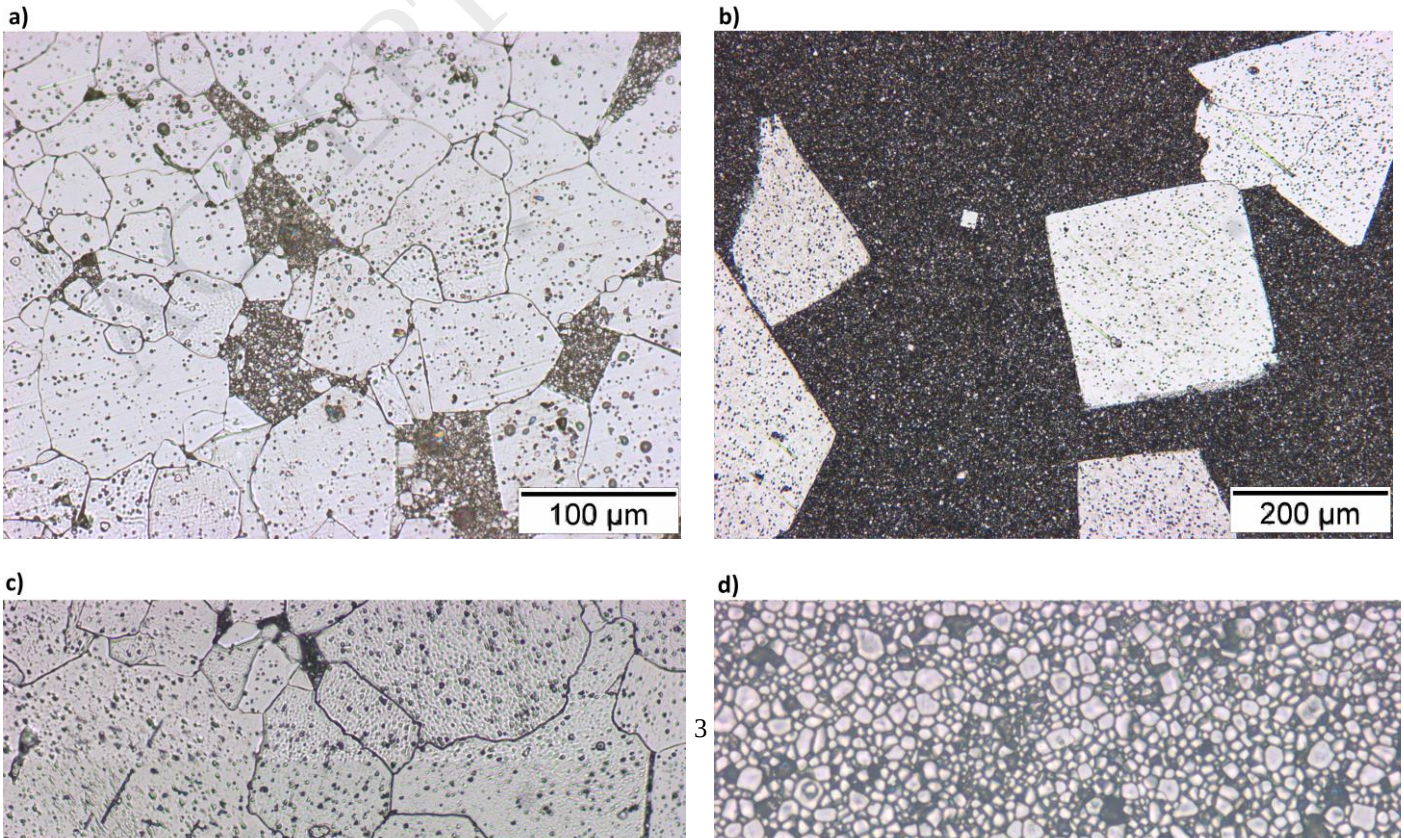

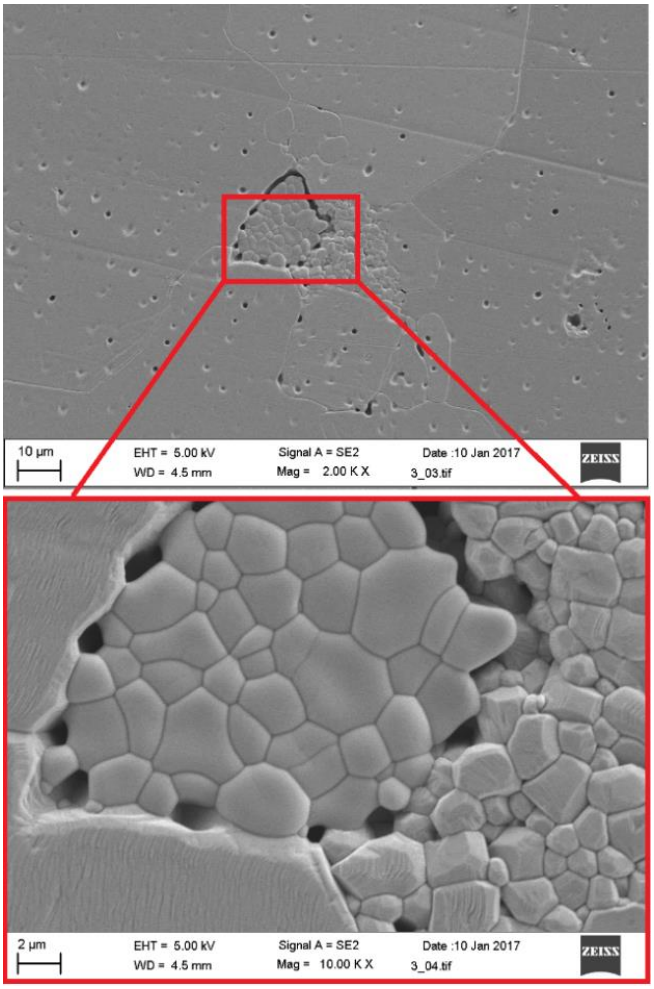

Figure 3. SEM micrographs of large grains growing from a contamination/inhomogeneity site.

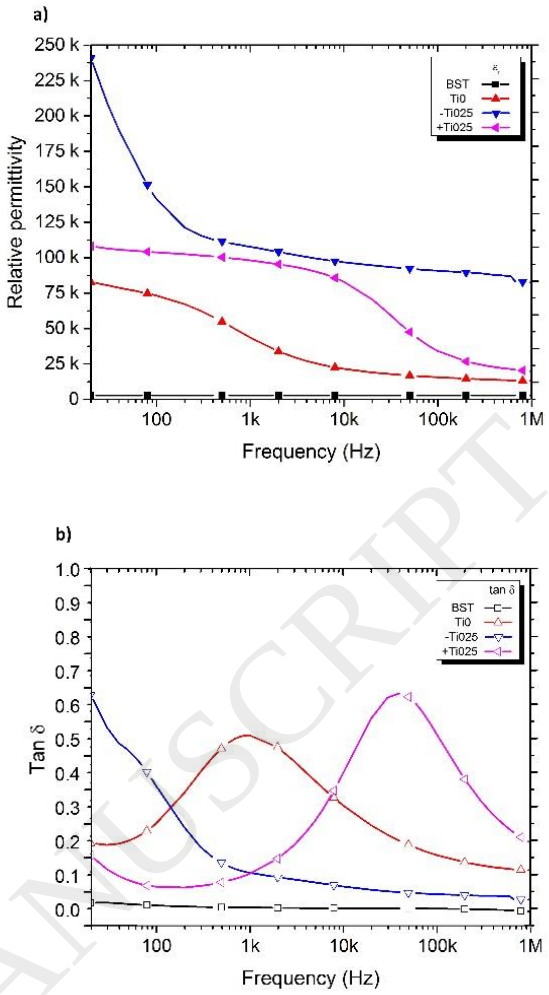

Figure 4 a) Relative permittivity and b) dielectric loss of sintered samples at room temperature.

introduction of La into the composition. Relative permittivity values started from 82,000 going through a relaxation at 0.1 - 10 kHz and ending at 13,000 at 1 MHz. Losses varied between 0.19 and 0.11 and peaked at 1 kHz. The –Ti025 sample displayed the highest relative permittivity overall and especially at low frequencies (240,000 at 20 Hz) which rapidly fell to a value around 100,000 at 500 Hz. Behaviour of the loss curve is similar to that of the permittivity, being high at low frequencies while decreasing to less than 0.05 between 30–40 kHz. High permittivity values at low frequencies can be due to the built-up of charge at the grain-grain boundary or electrode-sample interface which causes a large polarization [4]. The +Ti025 sample showed a similar behaviour to that of the Ti0 sample. The permittivity values started from >100,000 at low frequencies and went through a relaxation between 5 kHz and 120 kHz, finally settling at a value around 20,000. Losses varied from 0.062 to 0.63 peaking at a relaxation frequency 40 kHz.

The temperature dependent relative permittivity and dielectric loss curves for BST, Ti0, +Ti025 and -Ti025 samples at frequencies between 0.02 - 1000 kHz are displayed in Fig 5. In Fig. 5 a) and b) the temperature dependent dielectric properties are shown for the BST sample. A phase transition was observed as a sharp and well defined peak in permittivity (ε_r = 17,300, tan δ = 0.012) at T_c = -14 °C. This corresponds well with the findings of Alexandru et al. [21] and Fu et al. [22]. There were no major differences in dielectric values as a function of frequency except at low frequencies where the losses peaked and a small rise in permittivity was observed. This probably arose from space charge polarisation which is more pronounced at higher temperatures[23]. The Ti0 and +Ti025 samples in Fig 5. c) and e) showed colossal relative permittivity values, a strong broadening of the dielectric peak and suppression of the values as a function of frequency. The maximum permittivity values at 100 Hz for Ti0 and +Ti025 were 81,963 (T_{max} = -28 °C) and 102,985 (T_{max} = -16 °C), respectively. The temperature for maximum permittivity, T_{max}, shifted towards lower temperatures as the frequency increased. Dielectric losses for Ti0 showed a relaxation peak

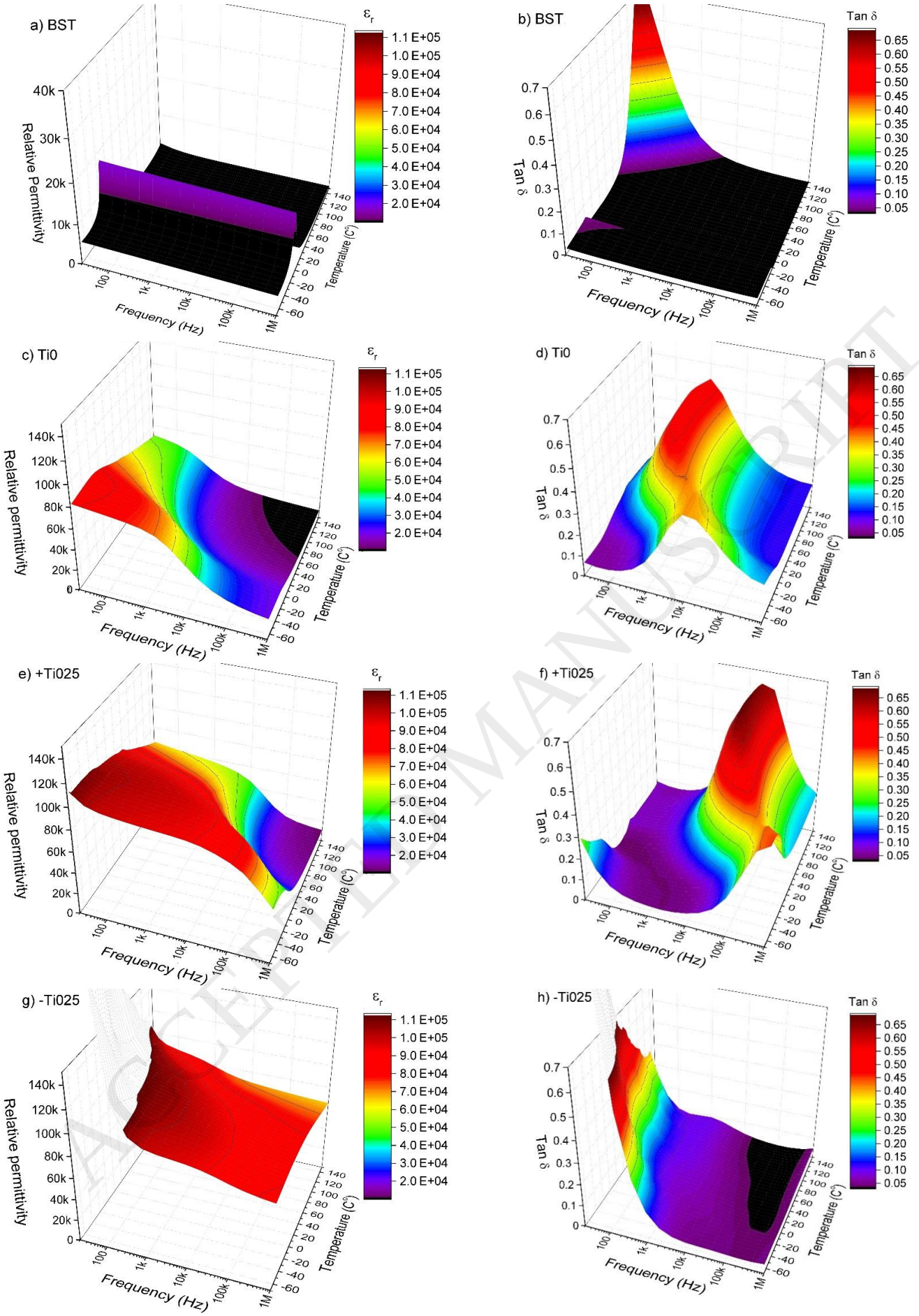

Figure 5. Temperature dependence of relative permittivity for a) BST, c) Ti0, e) +Ti025, g) -Ti025 and dielectric loss for b) BST, d) Ti0, f) +Ti025 and h) -Ti025 at various frequencies.

Table 2. Comparison between colossal permittivity materials.

Material	ε_r (x 10^4)	tan δ	Frequency range ($\varepsilon_r > 10^4$, tan δ < 0.05)	Temperature range ($\varepsilon_r > 10^4$, tan δ < 0.05)	Reference
$BaTi_{0.995}Nb_{0.005}O_3$ [a]	> 40000	-	$10^2 – 10^3$ Hz	-50 – 200 °C	[25]
$(Zn_{1/3}Nb_{2/3})_xTi_{1-x}O_2$	30000	0.2	$10 – 10^2$ Hz	-	[26]
$CaCu_3Ti_4O_{12}$ [b]	50000	0.35	40 – 1.5 x 10^3 Hz	-	[27]
$(Mg_{1/3}Ta_{2/3})_{0.05}Ti_{1-0.05}O_2$	15000	0.055	40 – 9 x 10^3 Hz	-	[28]
$Ba_{0.67}Sr_{0.33}TiO_3$ + 0.2 at.% La	110000	0.4	-	-100 – 200 °C	[4]
$Ba_{0.6}Sr_{0.4}TiO_3$ [c]	100000	> 0.5	20 – 4 x 10^3 Hz	37 – 122 °C	[7]
$(Ba_{0.54875}Sr_{0.44875}La_{0.0025})Ti_{0.9975}O_3$	87470	0.035	$10^4 – 10^6$ Hz	-68 – 150 °C	This work

[a] Sample annealed in N_2
[b] Sample fabricated by sol-gel technique
[c] Sample fabricated by SPS
Values approximated from reference graphs

at 10 kHz which shifted to 1 kHz at around the Curie point of the BST matrix composition (T_c = -14 °C). Similar behaviour was observed for the +Ti025 sample at around the BST Curie temperature. However, the point of highest losses for +Ti025 was obtained at 1000 kHz at -60 °C. This point shifted to around 20 kHz as the temperature increased, with a simultaneous increase of tan δ. The non-monotonic shift in the relaxation peak suggests a contribution from Maxwell-Wagner interfacial polarization[24]. The –Ti025 sample showed the highest relative permittivity values of all the compositions. The peak in permittivity (Fig. 5 g) was nearly flat between 1-1000 kHz. At 10 kHz the maximum relative permittivity was 98,360. Dielectric losses for –Ti025 were low compared to the Ti0 and +Ti025 samples in this frequency regime. No relaxation peaks were observed. At 10 kHz the sample exhibited a maximum tan δ of 0.0607. Both the permittivity and losses were relatively stable over a wide temperature range, above 1 kHz frequencies.

Table 2. shows the room temperature value of ε_r and tan δ as well as the frequency and temperature ranges, at which colossal permittivity is present, with industry acceptable losses in some cases (≤ 0.05)[3], for some of the recent colossal permittivity materials. Comparing –Ti25 to these recent colossal permittivity materials (Table 2.) it is apparent that over a wide higher frequency range ($10^4 – 10^6$ Hz) this composition is superior, both in relative permittivity and in dielectric losses.

4. Conclusion

All the BST samples with La addition exhibited colossal permittivity values >10^4. The addition of 0.25 mol.% of Ti stabilized the microstructure and increased the relative permittivity values up to 102,900 while keeping tan δ under 0.155 between 0.1 – 1 kHz. A shift in the relaxation peak towards lower frequencies was observed around the Curie temperature for sample +Ti025. A similar shift in the relaxation peak occurred in the sample without Ti modification, but at one decade lower frequency. Tan δ values were greater than 0.115 over the whole frequency and temperature range, except below 100 Hz and -26 °C where tan δ values were under 0.074. A more drastic difference was seen in the –Ti025 sample where permittivity values up to 98,360 and losses under 0.0607 were observed at frequencies over 10 kHz at temperatures between -68 °C to 150 °C.

As shown here, with fine adjustments of the composition, materials with colossal permittivity and relatively low dielectric losses with a wide range of frequency and temperature can be realized. The results are very encouraging for low loss colossal permittivity materials compared to recent BST-based [4,7] and other novel materials [1,3], [25–28], especially in the higher $10^4 – 10^6$ Hz frequency range. With further optimization a colossal permittivity material with a wider frequency range and lower losses with a dense microstructure could be achieved to be feasible for such as capacitor applications.

Acknowledgement

Authors Jari Juuti and Kari Nurmi gratefully acknowledges funding of the LEAP project from the Academy of Finland (grant agreement No. 267573, 273663 and 298409).

Data availability: The data that support the findings of this study are available from the corresponding author upon reasonable request

References

[1] W. Hu, Y. Liu, R.L. Withers, T.J. Frankcombe, L. Norén, A. Snashall, M. Kitchin, P. Smith, B. Gong, H. Chen, J. Schiemer, F. Brink, J. Wong-Leung, Electron-pinned defect-dipoles for high-performance colossal permittivity materials, Nat. Mater. 12 (2013) 821–826. doi:10.1038/nmat3691.

[2] Z. Valdez-Nava, C. Tenailleau, S. Guillemet-Fritsch, N. El Horr, T. Lebey, P. Dufour, B. Durand, J.Y. Chane-Ching, Structural characterization of dense reduced BaTiO3 and Ba 0.95La0.05TiO3 nanoceramics showing colossal dielectric values, J. Phys. Chem. Solids. 72 (2011) 17–23. doi:10.1016/j.jpcs.2010.10.016.

[3] S. De Almeida-Didry, C. Autret, A. Lucas, C. Honstettre, F. Pacreau, F. Gervais, Leading role of grain boundaries in colossal permittivity of doped and undoped CCTO, J. Eur. Ceram. Soc. 34 (2014) 3649–3654. doi:10.1016/j.jeurceramsoc.2014.06.009.

[4] J. Xu, H. Liu, B. He, H. Hao, M. Cao, High-permittivity and conduction mechanism of La-doped Ba0.67Sr0.33TiO3 ceramics, Phys. Status Solidi. 249 (2012) 1452–1458. doi:10.1002/pssb.201200001.

[5] H. Han, D. Ghosh, J.L. Jones, J.C. Nino, Colossal permittivity in microwave-sintered barium titanate and effect of annealing on dielectric properties, J. Am. Ceram. Soc. 96 (2013) 485–490. doi:10.1111/jace.12051.

[6] Z. Wang, M. Cao, Z. Yao, Q. Zhang, Z. Song, W. Hu, Q. Xu, H. Hao, H. Liu, Z. Yu, Giant permittivity and low dielectric loss of SrTiO3 ceramics sintered in nitrogen atmosphere, J. Eur. Ceram. Soc. 34 (2014) 1755–1760. doi:10.1016/j.jeurceramsoc.2014.01.015.

[7] S. Dupuis, S. Sulekar, J.H. Kim, H. Han, P. Dufour, C. Tenailleau, J.C. Nino, S. Guillemet-Fritsch, Colossal permittivity and low losses in Ba1-xSrxTiO3-δ reduced nanoceramics, J. Eur. Ceram. Soc. 36 (2016) 567–575. doi:10.1016/j.jeurceramsoc.2015.10.017.

[8] S. Rentsch, J. Mueller, Tunable dielectric material embedded in LTCC for GHz-frequency-range applications Tunable Dielectric Material Embedded in LTCC for, (2007).

[9] T. Hu, H. Jantunen, A. Uusim??ki, S. Lepp??vuori, Ba0.7Sr0.3TiO3 powders with B2O3 additive prepared by the sol-gel method for use as microwave material, Mater. Sci. Semicond. Process. 5 (2002) 215–221. doi:10.1016/S1369-8001(02)00074-4.

[10] J. Zhang, J. Zhai, X. Chou, X. Yao, Influence of rare-earth addition on microstructure and dielectric behavior of Ba0.6Sr0.4TiO3 ceramics, Mater. Chem. Phys. 111 (2008) 409–413. doi:10.1016/j.matchemphys.2008.04.050.

[11] C. ZHANG, Y. QU, Dielectric properties and phase transitions of La2O3- and Sb2O3-doped barium strontium titanate ceramics, Trans. Nonferrous Met. Soc. China. 22 (2012) 2742–2748. doi:10.1016/S1003-6326(11)61527-6.

[12] H. Zhao, Y. Li, C. Chang, C. Yan, Effects of La2O3-Doping and Sintering Temperature on the Dielectric Properties of BaSrTiO3 Ceramics, Mater. Res. 19 (2016) 474–477. doi:10.1590/1980-5373-MR-2016-0008.

[13] R.D. Shannon, Revised effective ionic radii and systematic studies of interatomic distances in halides and chalcogenides, Acta Crystallogr. Sect. A. (1976). doi:10.1107/S0567739476001551.

[14] R. T, G. R, B. B, Characterization of Barium Strontium Titanate Films Using XRD, Adv. X-Ray Anal. (1999) 38.

[15] M.N. Rahaman, Ceramic Processing and Sintering, 2nd ed., CRC Press, Boca Rato, FL, 2003.

[16] J.M. Saldaña, B. Mullier, G.A. Schneider, Preparation of BaTiO3 single crystals using the modified SiO2-exaggerated grain growth method, J. Eur. Ceram. Soc. 22 (2002) 681–688. doi:10.1016/S0955-2219(01)00336-3.

[17] H.-Y. Lee, J.-S. Kim, D.-Y. Kim, Fabrication of BaTiO3 single crystals using secondary abnormal grain growth, J. Eur. Ceram. Soc. 20 (2000) 1595–1597. doi:10.1016/S0955-2219(99)00197-1.

[18] J. Aguilar-Santillan, Wetting of Al2O3 by Molten Aluminum: The Influence of BaSO4 Additions, J. Nanomater. 2008 (2008) 1–12. doi:10.1155/2008/629185.

[19] R. Zhang, H. Mao, P. Taskinen, Thermodynamic descriptions of the BaO-CaO, BaO-SrO, BaO-SiO2 and SrO-SiO2 systems, Calphad Comput. Coupling Phase Diagrams Thermochem. 54 (2016) 107–116. doi:10.1016/j.calphad.2016.06.009.

[20] M. Drofenik, D. Makovec, I. Zajc, H.T. Langhammer, Anomalous Grain Growth in Donor-Doped Barium Titanate with Excess Barium Oxide, J. Am. Ceram. Soc. 85 (2004) 653–660. doi:10.1111/j.1151-2916.2002.tb00146.x.

[21] H. V. Alexandru, C. Berbecaru, A. Ioachim, L. Nedelcu, A. Dutu, BST solid solutions, temperature evolution of the ferroelectric transitions, Appl. Surf. Sci. 253 (2006) 354–357. doi:10.1016/j.apsusc.2006.06.011.

[22] C. Fu, C. Yang, H. Chen, Y. Wang, L. Hu, Microstructure and dielectric properties of BaxSr1−xTiO3 ceramics, Mater. Sci. Eng. B. 119 (2005) 185–188. doi:10.1016/j.mseb.2005.02.056.

[23] A.M. Badr, H.A. Elshaikh, I.M. Ashraf, Impacts of Temperature and Frequency on the Dielectric Properties for Insight into the Nature of the Charge Transports in the Tl 2 S Layered Single Crystals, 2011 (2011) 12–25. doi:10.4236/jmp.2011.21004.

[24] H. Dong, W. Ying, M. Ji-Yuan, L. Zhi-Fu, L. Yong-Xiang, Colossal Permittivity and Dielectric Relaxations of (Nb, Al)Co-doped BaTiO$lt;inf$gt;3$lt;/inf$gt; Ceramics, J. Inorg. Mater. 32 (2017) 219. doi:10.15541/jim20160280.

[25] P. Ren, J. He, X. Wang, M. Sun, H. Zhang, G. Zhao, Colossal permittivity in niobium doped BaTiO3ceramics annealed in N2, Scr. Mater. 146 (2018) 110–114. doi:10.1016/j.scriptamat.2017.11.026.

[26] N. Thongyong, W. Tuichai, N. Chanlek, P. Thongbai, Effect of Zn2+and Nb5+co-doping ions on giant dielectric properties of rutile-TiO2ceramics, Ceram. Int. 43 (2017) 15466–15471. doi:10.1016/j.ceramint.2017.08.093.

[27] Z. Peng, P. Liang, X. Wang, H. Peng, X. Chen, Z. Yang, X. Chao, Fabrication and characterization of CdCu3Ti4O12ceramics with colossal permittivity and low dielectric loss, Mater. Lett. 210 (2018) 301–304. doi:10.1016/j.matlet.2017.09.041.

[28] W. Dong, D. Chen, W. Hu, T.J. Frankcombe, H. Chen, C. Zhou, Z. Fu, X. Wei, Z. Xu, Z. Liu, Y. Li, Y. Liu, Colossal permittivity behavior and its origin in rutile (Mg1/3Ta2/3)xTi1-xO2, Sci. Rep. 7 (2017) 1–8. doi:10.1038/s41598-017-0899

Figure Caption

Figure 1. XRD patterns for sintered samples.

Figure 2. Microstructure of sintered samples. a) BST b) -Ti025, c) Ti0 and d) +Ti025.

Figure 3. SEM micrographs of large grains growing from a contamination/inhomogeneity site.

Figure 4 a) Relative permittivity and b) dielectric loss of sintered samples at room temperature.

Figure 5. Temperature dependence of relative permittivity for a) BST, c) Ti0, e) +Ti025, g) -Ti025 and dielectric loss for b) BST, d) Ti0, f) +Ti025 and h) -Ti025 at various frequencies.

Table 1. Sample densities and average grain sizes.
Table 2. Comparison between colossal permittivity materials.